SANDIA REPORT

SAND2019-10308
Unlimited Release
Printed

SPARC Simulations of CUBRC Experiment Run 34 of the HIFiRE-1 Vehicle

V. Gregory Weirs

Prepared by
Sandia National Laboratories
Albuquerque, New Mexico 87185 and Livermore, California 94550

Sandia National Laboratories is a multimission laboratory managed and operated by National Technology and Engineering Solutions of Sandia, LLC., a wholly owned subsidiary of Honeywell International, Inc., for the U.S. Department of Energy's National Nuclear Security Administration under contract DE-NA0003525.

Sandia National Laboratories

Issued by Sandia National Laboratories, operated for the United States Department of Energy by National Technology and Engineering Solutions of Sandia, LLC.

Available to DOE and DOE contractors from
U.S. Department of Energy
Office of Scientific and Technical Information
P.O. Box 62
Oak Ridge, TN 37831

Telephone: (865) 576-8401
Facsimile: (865) 576-5728
E-Mail: reports@adonis.osti.gov
Online ordering: http://www.osti.gov/bridge

Available to the public from
U.S. Department of Commerce
National Technical Information Service
5285 Port Royal Rd
Springfield, VA 22161

Telephone: (800) 553-6847
Facsimile: (703) 605-6900
E-Mail: orders@ntis.fedworld.gov
Online ordering: http://www.ntis.gov/help/ordermethods.asp?loc=7-4-0#online

SAND2019-10308
Unlimited Release
Printed

SPARC Simulations of CUBRC Experiment Run 34 of the HIFiRE-1 Vehicle

V. Gregory Weirs
Scientific Computation Department
Sandia National Laboratories
P.O. Box 5800, MS 1320
Albuquerque, NM 87185-1320
vgweirs@sandia.gov

Abstract

This report describes numerical simulations of CUBRC HIFiRE-1 ground test experiment Run 34 produced by SPARC.

Contents

Chapter 1

Summary

Ground test experiments of the HIFiRE-1 vehicle were carried out at Calspan University of Buffalo Research Center (CUBRC) and were described in [2]. In this report the focus is on the experiment labeled Run 34, which corresponds to "Condition B" in [2]. The freestream conditions are $M_\infty = 7.092$, $u_\infty = 2168.7$m/s, $T_\infty = 231.91$K, $p_\infty = 4.069$kPa, and $\rho_\infty = 0.070215$kg/m^3. The wall temperature was $T_w = 296.6$K, and the model is mounted in the tunnel at 2^o angle of attack.

The Run 34 experiment was simulated with SPARC [1]. A sequence of 3D, half-symmetry meshes were generated in the commercial software Pointwise, with the coarsest mesh have around 2 million elements. The mesh itself is symmetric about x-z plane, and the angle of attack is expressed by adjusting the inflow velocity direction. Simulations on these meshes use a perfect gas model for air, Sutherland model for viscosity, and Menter Shear Stress Transport (SST) model for turbulence. From an initial condition defined by the freestream conditions, the steady state solution is obtained by through an iterative approach.

The simulations produce output including the flowfield variables (density, temperature, pressure, velocity, turbulent viscosity) and data on the body surface, such as heat flux, skin friction, etc. The results also include diagnostics of the simulation, such as information on the time step, convergence rate, and solution residuals.

The following figures show several flowfield variables on slices of the domain. Figures 1.1, 1.2, 1.3, 1.4, and 1.5, present the Mach number, density, pressure, temperature, and turbulent viscosity, respectively, in the symmetry (x, y, $z = 0$) plane. At 2 degrees AoA, flow is from left to right from just below the centerline. While very similar, the shock structure and strength are visibly different on the windward and leeward sides of the body. The largest visible differences are near the cylinder-flare intersection, where flow separation occurs further upstream on the leeward side which significantly affects the local shock structure and impingement on the body.

A close up of the flow near the nose is shown in Figs. 1.6(a), 1.6(b), 1.7(a), and 1.7(b). The strong bow shock leads to the highest densities, pressures, and temperatures in the flowfield.

Figures 1.8, 1.9, 1.10, 1.11, and 1.12, present the Mach number, density, pressure, temperature, and turbulent viscosity, respectively, in several cross-sectional planes. The first

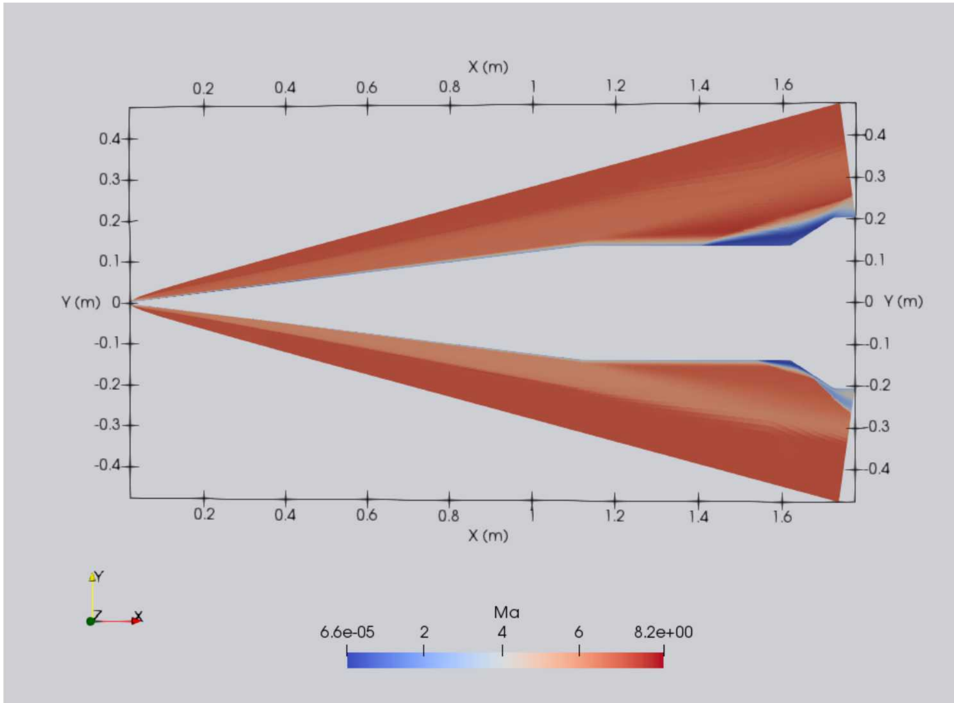

Figure 1.1. Mach number in the symmetry plane.

plane is in a laminar region, just upstream of where the flow is tripped in the simulation. The third plane is at the boundary of the forecone and the cylinder, and the second plane is midway between the first and third planes. Finally, the fourth plane is at the cylinder-flare intersection. These figures illustrate that significant 3D effects in the flow near the cylinder-flare intersection.

Figure 1.13 shows the density (log scale) in the y-z plane at the end of the flare, and the wall heat flux on the cylinder and flare on a wireframe mesh. On the windward side of the body (lower side in the figure), the separation region is smaller and the separation shock and its interactions with the shock from the flare are closer to the body; the transmitted shock impinges on the flare leading to large localized heating. Going around the body to the leeward side, flow separation moves upstream, the separation bubble gets bigger, and the shock impingement moves off the flare.

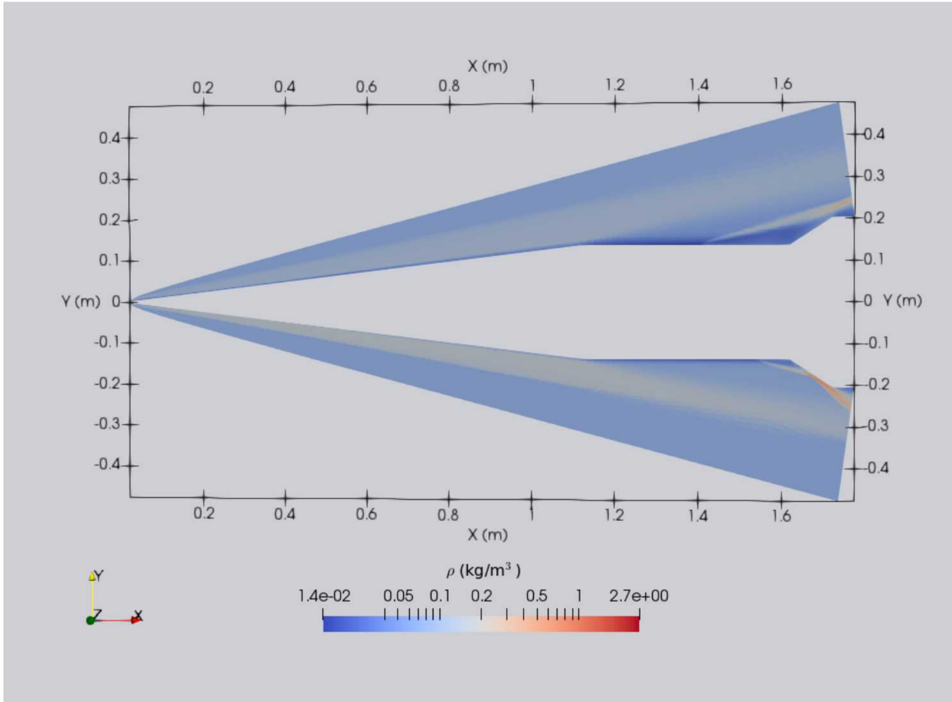

Figure 1.2. Density (log scale) in the symmetry plane.

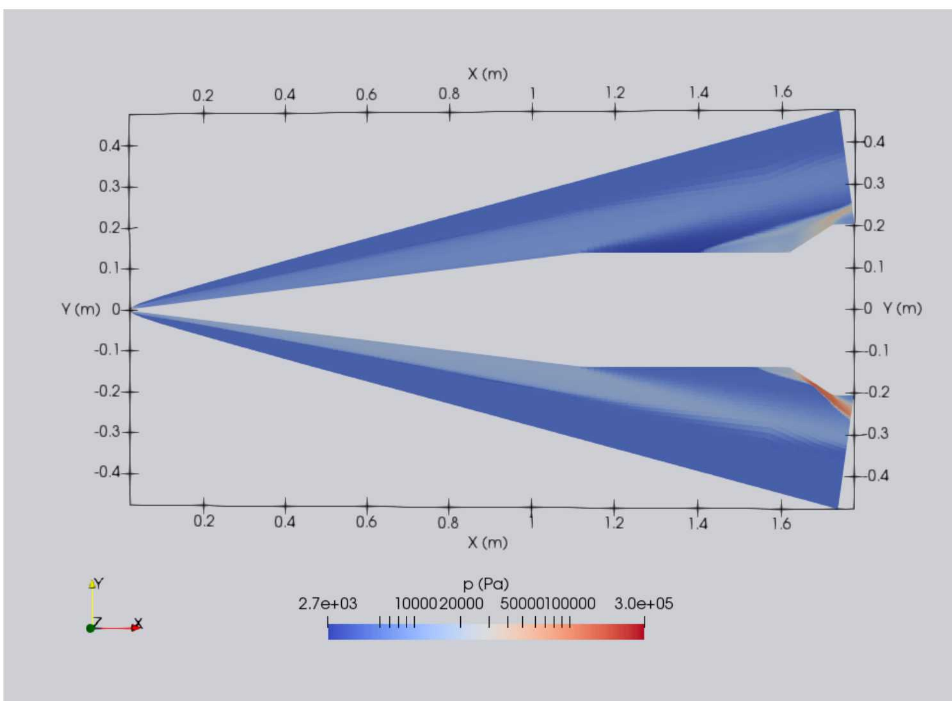

Figure 1.3. Pressure (log scale) in the symmetry plane.

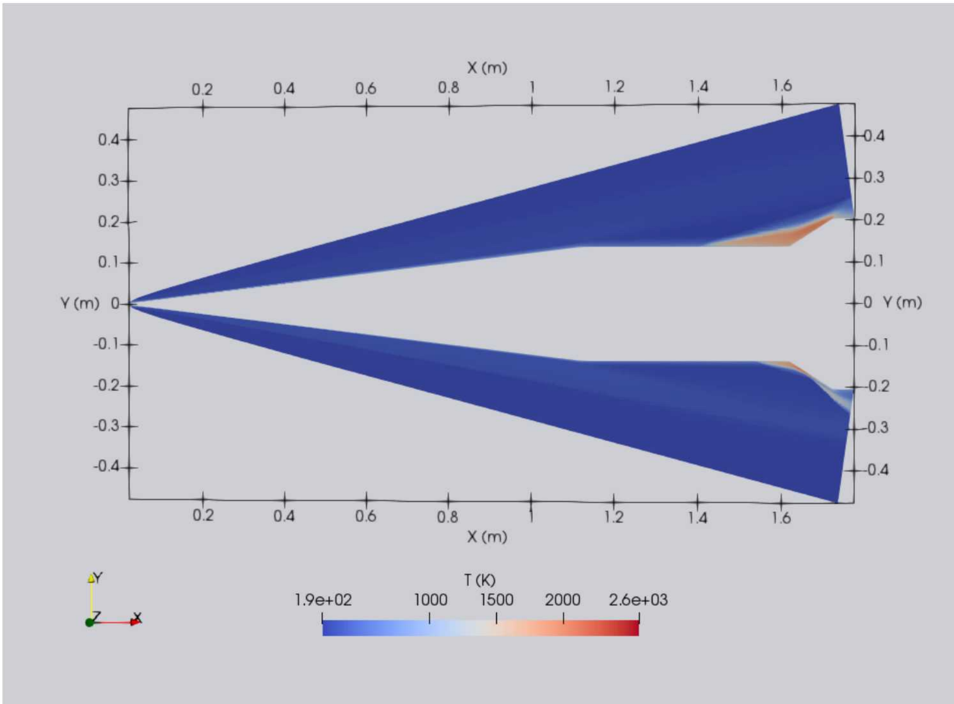

Figure 1.4. Temperature in the symmetry plane.

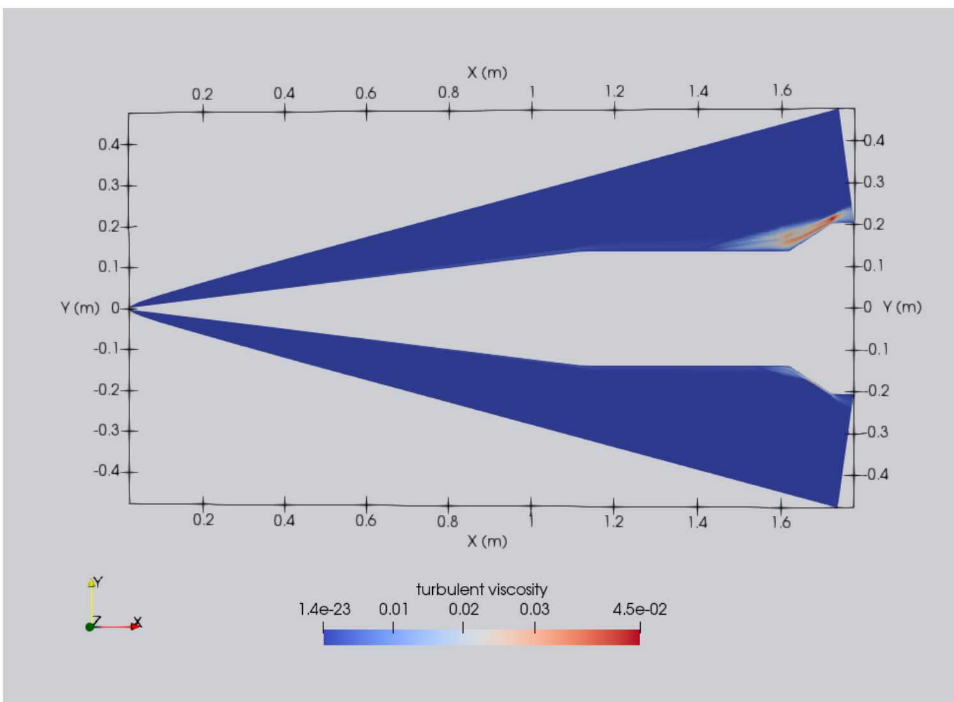

Figure 1.5. Turbulent viscosity in the symmetry plane.

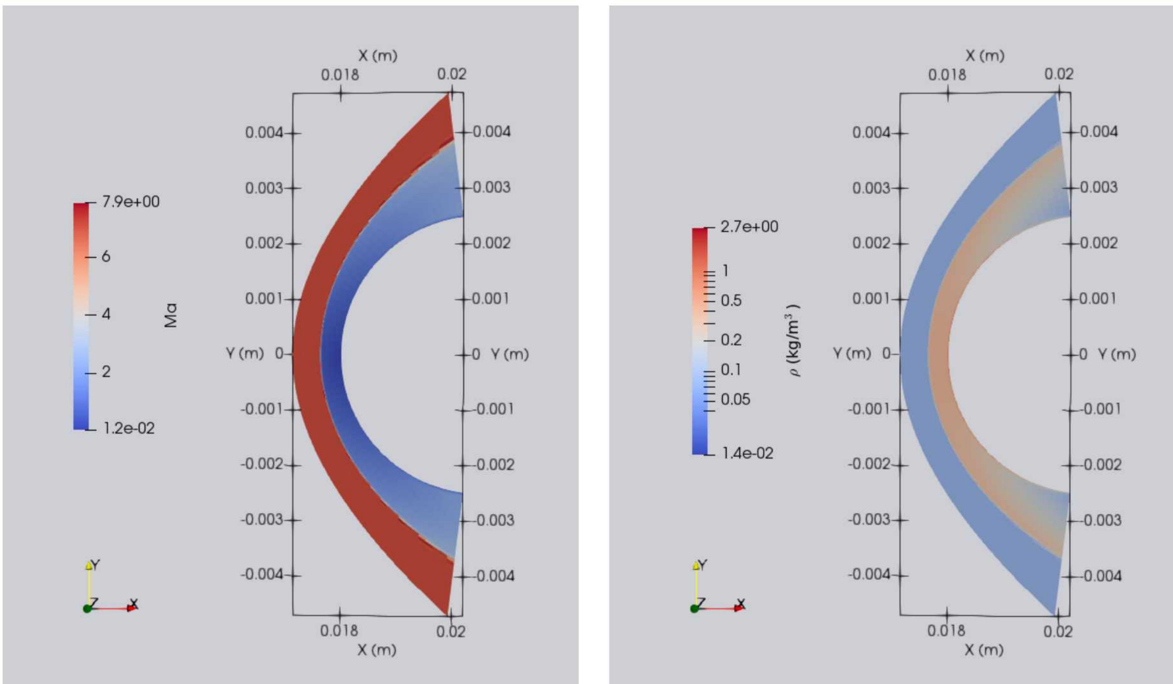

(a) Mach number **(b)** Density (log scale)

Figure 1.6. Mach number and density near the nose.

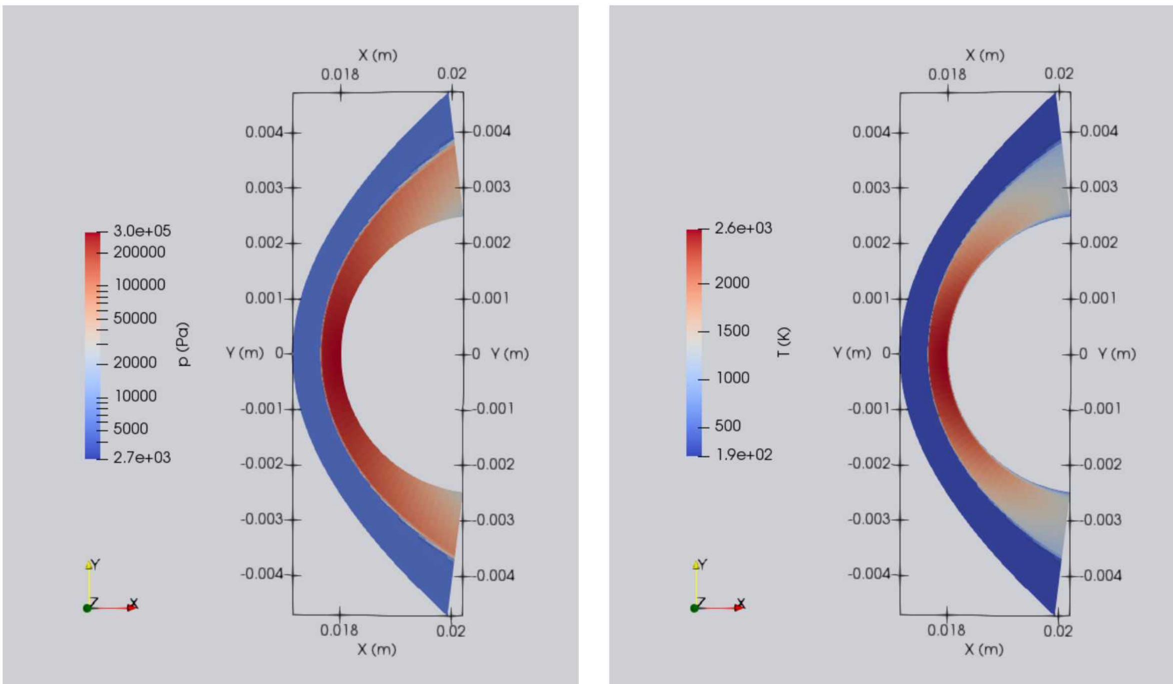

(a) Pressure (log scale)

(b) Temperature

Figure 1.7. Pressure (log scale) and temperature near the nose.

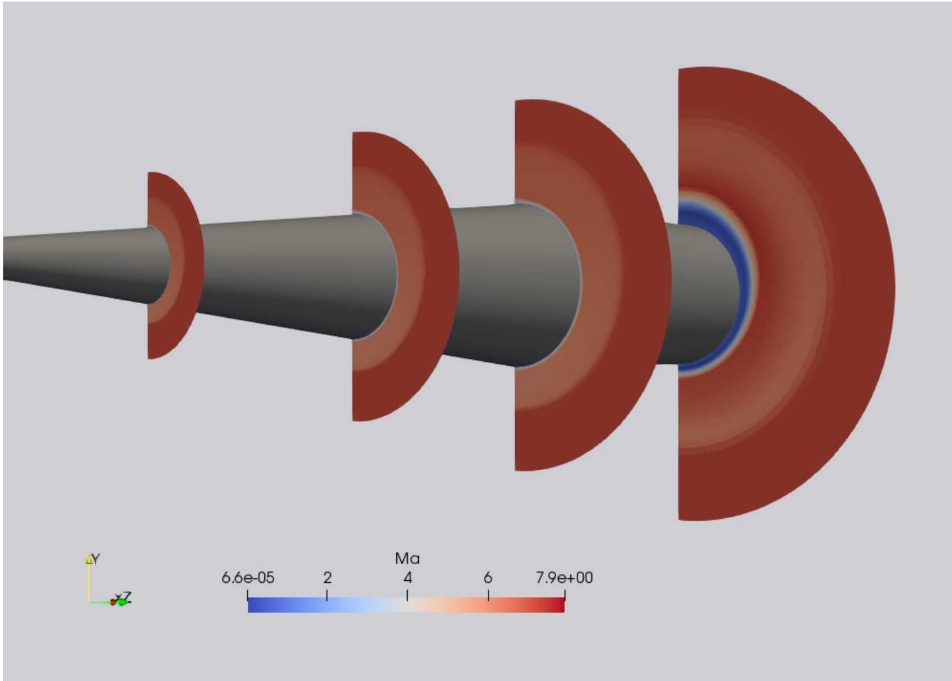

Figure 1.8. Mach number in several x-z planes.

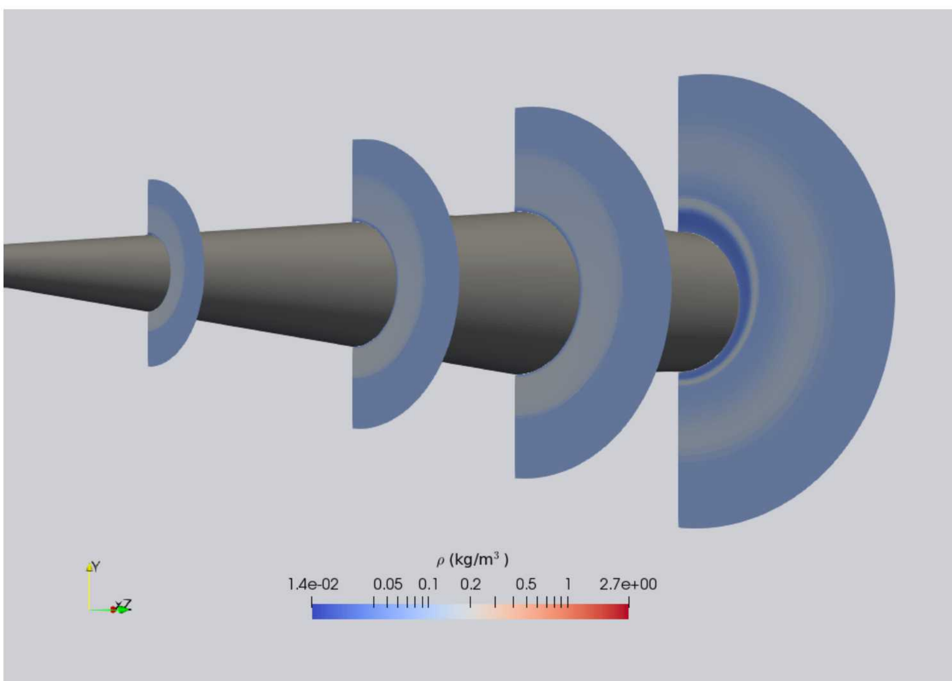

Figure 1.9. Density (log scale) in several x-z planes.

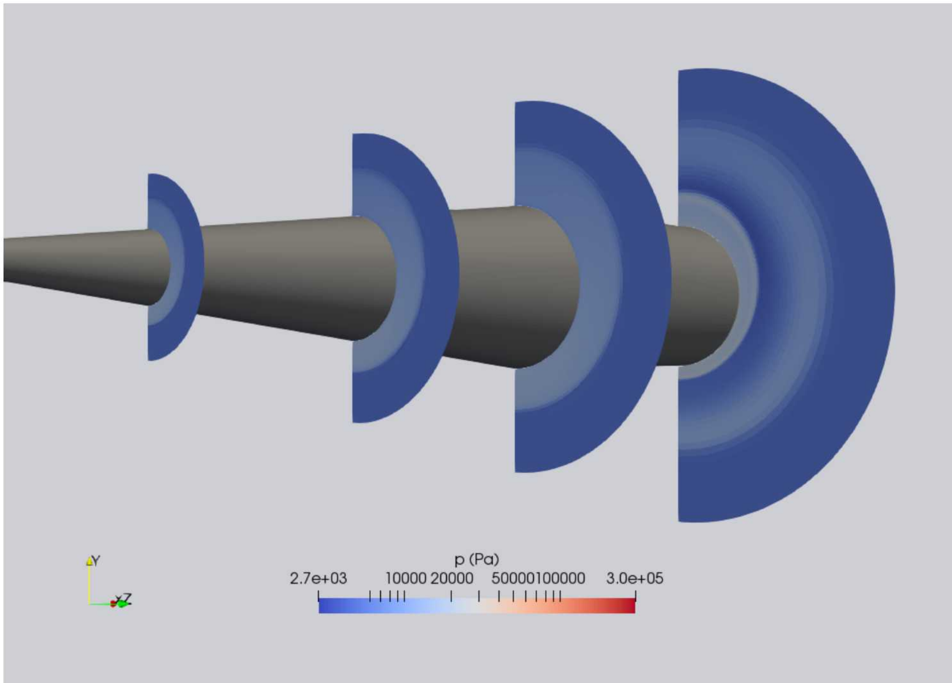

Figure 1.10. Pressure (log scale) in several x-z planes.

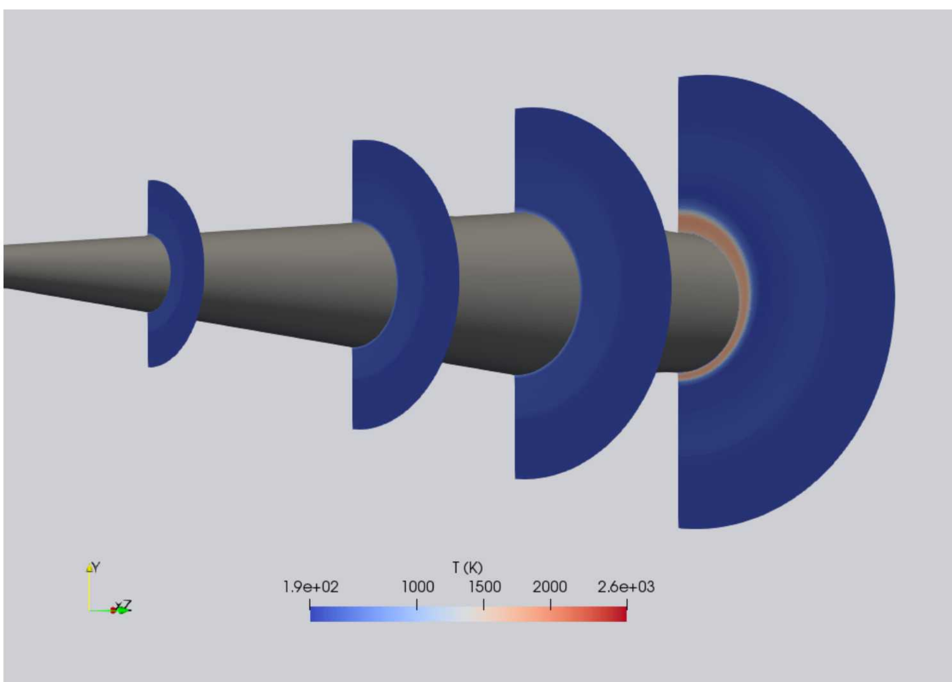

Figure 1.11. Temperature in several x-z planes.

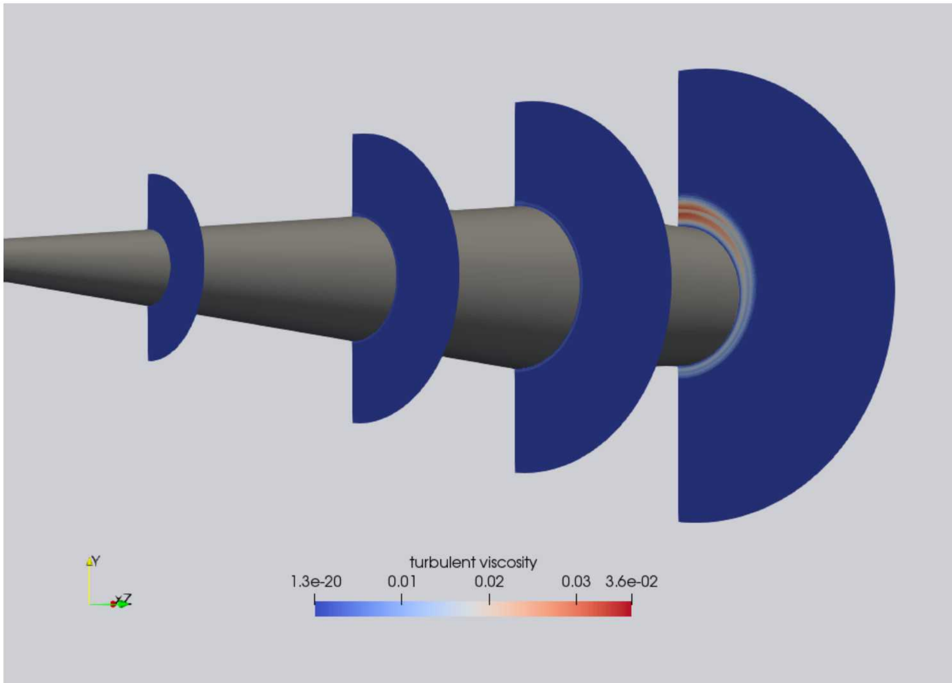

Figure 1.12. Turbulent viscosity in several x-z planes.

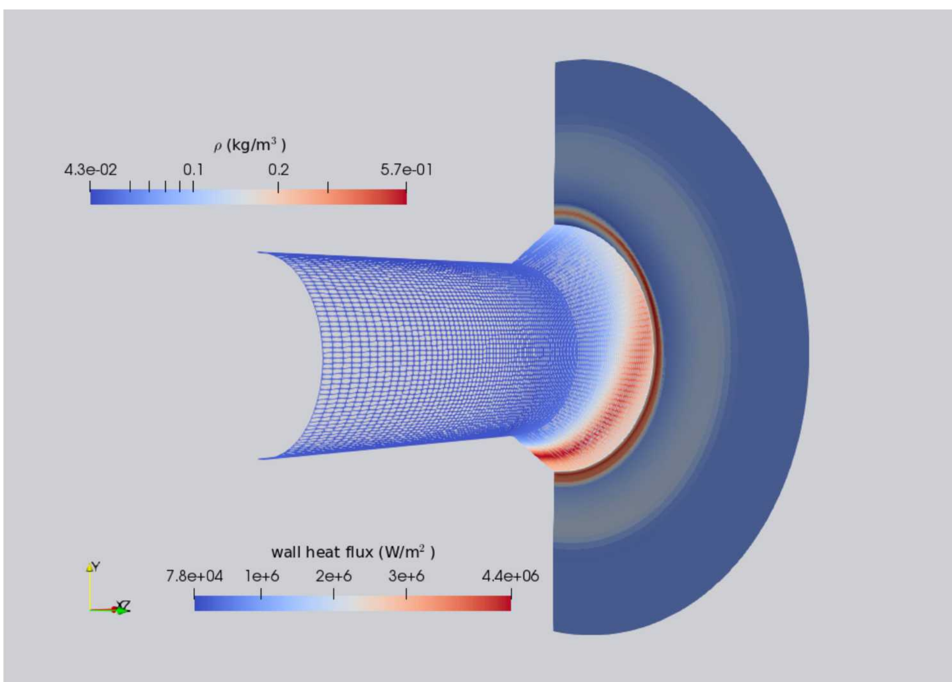

Figure 1.13. Localized heating on the flare.

References

[1] M. Howard, A. M. Bradley, W. W. Bova, J. R. Overfelt, R. M. Wagnild, D. J. Dinzl, M. F. Hoemmen, and A. M. Klinvex. Towards a performance portable compressible cfd code. In *23rd AIAA Computational Fluid Dynamics Conference, AIAA Aviation 2017 (AIAA-2017-4407)*, 2017.

[2] T. P. Wadhams, E. Mundy, M. G. MacLean, and M. S. Holden. Ground test studies of the HIFiRE-1 transition experiment Part 1: Experimental results. *Journal of Spacecraft and Rockets*, 45(6):1134–1148, 2008.

DISTRIBUTION:

	MS	,
		,
1	MS 0899	Technical Library, 9536 (electronic copy)

v1.40

Sandia National Laboratories